Journal of Alloys and Compounds 500 (2010) 215–219

Contents lists available at ScienceDirect

Journal of Alloys and Compounds

journal homepage: www.elsevier.com/locate/jallcom

Synthesis and thermoelectric properties of $Zn_4Sb_3/Bi_{0.5}Sb_{1.5}Te_3$ bulk nanocomposites

J.H. Sun, X.Y. Qin*, H.X. Xin, D. Li, L. Pan, C.J. Song, J. Zhang, R.R. Sun, Q.Q. Wang, Y.F. Liu

Key Laboratory of Materials Physics, Institute of Solid State Physics, Chinese Academy of Sciences, 230031 Hefei, China

ARTICLE INFO

Article history:
Received 21 January 2010
Received in revised form 29 March 2010
Accepted 2 April 2010
Available online 9 April 2010

Keywords:
Semiconductor
Nanocomposite
Thermoelectric
Hot-pressing

ABSTRACT

The bulk nanocomposites $f(Zn_4Sb_3)/Bi_{0.5}Sb_{1.5}Te_3$ (f = 0, 5, 10 and 15 vol.%) were prepared, and their thermoelectric properties were investigated at temperatures from 300 to 650 K. The results of X-ray diffraction (XRD) and field emission scanning electron microscopy (FE-SEM) showed that the nanometer-sized Zn_4Sb_3 particles were dispersed homogeneously in $Bi_{0.5}Sb_{1.5}Te_3$ matrix. Transport property measurements indicated that the resistivity and Seebeck coefficient of the composite samples $f(Zn_4Sb_3)/Bi_{0.5}Sb_{1.5}Te_3$ (f = 0, 5, 10 and 15 vol.%) decreased with increasing Zn_4Sb_3 content due to the increase in carrier concentration. Experiments also showed that thermal conductivity of $f(Zn_4Sb_3)/Bi_{0.5}Sb_{1.5}Te_3$ decreased monotonically with increasing f owing to enhanced phonon scattering by the dispersed Zn_4Sb_3 nanoparticles and the phase boundaries in the matrix. Among the samples studied, 15 vol.% $(Zn_4Sb_3)/Bi_{0.5}Sb_{1.5}Te_3$ exhibited the largest power factor (25 $\mu W/cm\,K^2$ at ~300 K) that was 2.5 times larger than that of $Bi_{0.5}Sb_{1.5}Te_3$; correspondingly, its figure of merit (ZT = 0.6 at ~300 K) was about three times larger than that of $Bi_{0.5}Sb_{1.5}Te_3$, indicating that the thermoelectric properties of $Bi_{0.5}Sb_{1.5}Te_3$ can be enhanced effectively by the dispersion of nanometer-sized Zn_4Sb_3.

1. Introduction

Pseudo-binary alloys p-type $(Bi_2Te_3)_{1-x}(Sb_2Te_3)_x$ (x = 0.75) and n-type $(Bi_2Te_3)_{1-y}(Bi_2Se_3)_y$ (y = 0.1) are the best thermoelectric (TE) materials around the room temperature [1]. Numerous researches have been performed to enhance the figure of merit, $ZT = S^2T/\rho\lambda$ (where S is the Seebeck coefficient, ρ is the electrical resistivity, λ is the thermal conductivity, and T is the absolute temperature) by alloying and doping [2–10] since Bi_2Te_3-based thermoelectric materials were found in 1950s. Recent reports, however, demonstrate that low-dimensional TE materials such as p-type Bi_2Te_3/Sb_2Te_3 superlattice thin films [11,12] and the nanostructured $(Bi, Sb)_2Te_3$ bulk alloys [13–15] show a significant enhancement of their ZT mainly due to decreases of the thermal conductivity in these structures. Especially, experimental works on Bi_2Te_3-alloy based nanocomposites indicate that both a decrease in thermal conductivity and an increase in the power factor (S^2/ρ) are possible in nanocomposite systems [16–19].

Since β-Zn_4Sb_3 possesses high figure of merit in the moderate temperature (ZT = 1.3 at 673 K) [20,21] due to its extremely low thermal conductivity, it is expected that the combination of $Bi_{0.5}Sb_{1.5}Te_3$ (matrix) with Zn_4Sb_3 (dispersed phase) will produce a composite system with better thermoelectric properties. Hence, in present work $Bi_{0.5}Sb_{1.5}Te_3$-based (nano)composites dispersed with nanometer-sized Zn_4Sb_3 particles were fabricated, and their thermoelectric properties were evaluated and discussed in relevant to their microstructures.

2. Experimental procedures

$(Zn_4Sb_3)/Bi_{0.5}Sb_{1.5}Te$ nanocomposite samples were fabricated by using a method of vacuum melting and ball milling, followed by a vacuum hot-pressing. In order to obtain p-type $Bi_{0.5}Sb_{1.5}Te_3$ and β-phase Zn_4Sb_3 compounds, constituent elements Bi (4N), Sb (3N) and Te (4N) (for $Bi_{0.5}Sb_{1.5}Te_3$), and (Zn (5N) and Sb (3N)) (for Zn_4Sb_3) were separately sealed into evacuated quartz tubes corresponding to their stoichiometry. Firstly, for the synthesis of $Bi_{0.5}Sb_{1.5}Te_3$ alloy the mixture of the constituent elements were melted at 973 K and isothermally kept for 6 h before cooling to room temperature; while for the synthesis of Zn_4Sb_3 compound the mixture of elements Zn and Sb were heated slowly to 1023 K and isothermally kept for 12 h before quenching in water. Secondly, in order to obtain nanometer-sized powders of $Bi_{0.5}Sb_{1.5}Te_3$ and Zn_4Sb_3 alloys, the obtained $Bi_{0.5}Sb_{1.5}Te_3$ and Zn_4Sb_3 alloys ingots (rod) were ground into pieces and then were ball-milled respectively in a high-energy planetary mill (QM-SB) with a speed of 260 rmp under Ar atmosphere for 50 h (nano-$Bi_{0.5}Sb_{1.5}Te_3$) and 40 h (nano-Zn_4Sb_3). Thirdly, the nanometer-sized Zn_4Sb_3 and $Bi_{0.5}Sb_{1.5}Te_3$ powders were mixed for 5 h with a planetary mill in accordance with the volume ratio of 5:95, 10:80 and 15:75 at a speed of 150 rmp. Finally, the obtained powder samples were then compacted by hot-pressing in vacuum under the pressure of 600 MPa at 623 K for 1 h to form bulk nanocomposite samples. The phase structures of the samples were investigated by using X-ray diffraction (XRD) (Philips-X PERT PRO diffractometer) with CuK_α radiation. The average grain sizes of samples were estimated using Scherrer formula and confirmed by using field emission scanning electron microscopy (FE-SEM). The microstructures of the nanocomposite samples were revealed by using back-scattered electron (BSE)

* Corresponding author. Tel.: +86 551 5592750; fax: +86 551 5591434.
E-mail address: xyqin@issp.ac.cn (X.Y. Qin).

0925-8388/$ – see front matter © 2010 Elsevier B.V. All rights reserved.
doi:10.1016/j.jallcom.2010.04.006

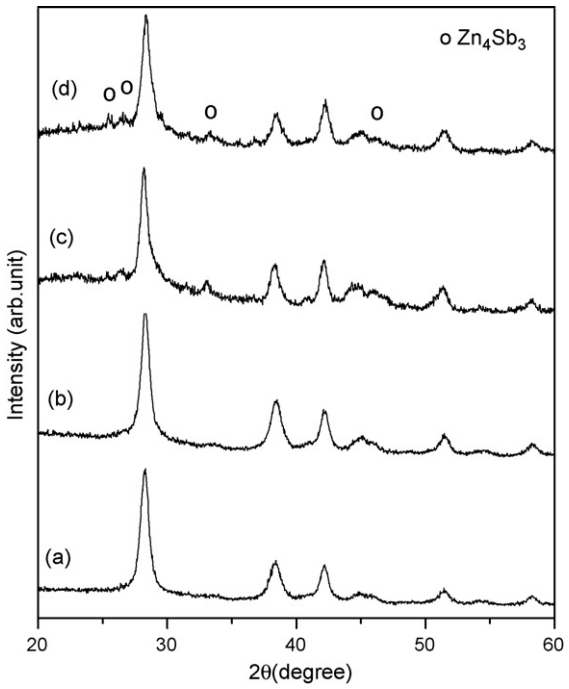

Fig. 1. XRD patterns (Cu K_α irradiation) of $f(Zn_4Sb_3)/Bi_{0.5}Sb_{1.5}Te_3$: (a) $f = 0$, (b) $f = 5$, (c) $f = 10$ and (d) $f = 15$ vol.% at room temperature.

images obtained with the FE-SEM. The compositions and the constituent phases of the synthesized nanocomposites were confirmed by using energy dispersive analysis system of X-ray (EDX) equipped in FE-SEM. Hall coefficient was measured at 293 K by applying a field of 0.73 T, and the carrier concentrations and mobility were calculated by using Hall coefficient and electrical resistivity. The electrical resistivity and Seebeck coefficient were measured simultaneously by the standard four-probe method (ULVAC-RIKO: ZEM-3, Japan) under He atmosphere from 300 to 650 K. The thermal conductivity was measured by using a physical property measurement system (PPMS, Quantum Design).

3. Results and discussion

3.1. Microstructural characterization

Fig. 1 shows XRD patterns for $f(Zn_4Sb_3)/Bi_{0.5}Sb_{1.5}Te_3$ composite samples with different Zn_4Sb_3 contents ($f = 0$, 5, 10 and 15 vol.%). It is noted that no obvious impurity phase could be detected; that is, there are only two phases in these nanocomposite samples: one is Zn_4Sb_3 and the other is $Bi_{0.5}Sb_{1.5}Te_3$. In addition, it is observed that Zn_4Sb_3 phase becomes increasingly evident with the increase of Zn_4Sb_3 content. In Fig. 1 the diffraction peaks of the XRD patterns for all the specimens broaden substantially. This broadening of the diffraction peaks indicates the refinement of grain size of the samples. The average grain size of both phases estimated by using the Scherrer formula is around 20–50 nm. This is well in agreement with FE-SEM observations, as shown in Fig. 2 which shows that most of the particles in the fracture surface of 10 vol.% $(Zn_4Sb_3)/Bi_{0.5}Sb_{1.5}Te_3$ sample have the sizes <100 nm (considering that some agglomeration is inevitable in the observed fracture surface).

The morphologies of the microstructures for $f(Zn_4Sb_3)/Bi_{0.5}Sb_{1.5}Te_3$ ($f = 5$, 10 and 15 vol.%) nanocomposite samples are revealed by using BSE images obtained with the FE-SEM, as presented in Fig. 3. One can see that the common feature for these morphologies is the embedded black spots (particles) on a white background. EDX analysis shows that these black particles belong to Zn rich phase and the white continuous background belongs to Bi rich phase (Fig. 3d and e). Hence, these black spots are actually the dispersed phase Zn_4Sb_3 (as marked in the graphs)

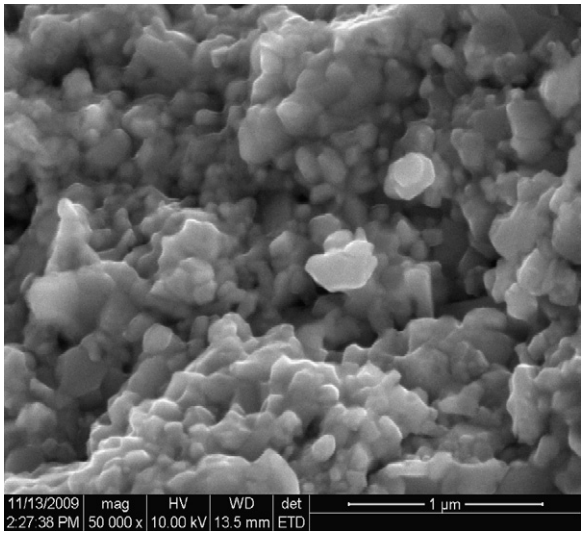

Fig. 2. Scanning electron micrographs (secondary electron image) of grains for 10 vol.% $(Zn_4Sb_3)/Bi_{0.5}Sb_{1.5}Te_3$ bulk specimen.

and they are dispersed homogeneously in $Bi_{0.5}Sb_{1.5}Te_3$ matrix (the white background). By comparison, one can find that the more of the Zn_4Sb_3 content, the denser of the Zn_4Sb_3 particles (black spots) on the observed fracture surfaces. In addition, by careful inspection one can see that the black spots are actually agglomerates of Zn_4Sb_3 grains with nanometer sizes (see the inset in Fig. 3c), and these agglomerates become bigger with increasing Zn_4Sb_3 content. But, it is worthwhile to point out that the space resolution of BSE images is not high enough to detect the monodispersed nano-Zn_4Sb_3 particles or distinguish the agglomerates smaller than ~100 nm from the BiSbTe matrix. We expect that it is these highly dispersed Zn_4Sb_3 particles that play a decisive role in influencing the electrical transport and thermoelectric properties of the composite system (see the next section).

3.2. The resistivity and Seebeck coefficient

The variations of electrical resistivity of $f(Zn_4Sb_3)/Bi_{0.5}Sb_{1.5}Te_3$ ($f = 0$, 5, 10 and 15 vol.%) nanocomposite samples with temperature are shown in Fig. 4. The temperature behavior of the electrical resistivity for the four samples are similar: the electrical resistivity increases initially with increasing the temperature and then decreases with further increasing temperature, leaving a maximum locating at a particular temperature T_{max} [$T_{max} = 325$, 425 and 550 K for $f(Zn_4Sb_3)/Bi_{0.5}Sb_{1.5}Te_3$ with $f = 0$, 5 and 10 vol.%, respectively. The T_{max} of the 15 vol.% $(Zn_4Sb_3)/Bi_{0.5}Sb_{1.5}Te_3$ is expected to be higher than 550 K, which is beyond the temperature range of our measurements]. At the temperatures above T_{max}, the electrical resistivity for the four samples decreases with further increasing temperature. This reduction in electrical resistivity is mainly due to the onset of mixed conduction [22] in $Bi_{0.5}Sb_{1.5}Te_3$. It is noted that the onset temperature of mixed conduction shifts from 325 K for $Bi_{0.5}Sb_{1.5}Te_3$ to 550 K for 10 vol.% $(Zn_4Sb_3)/Bi_{0.5}Sb_{1.5}Te_3$. The shift of T_{max} (corresponding to the onset of mixed conduction) toward higher temperatures with increasing Zn_4Sb_3 content (Fig. 4) indicates that the addition of the Zn_4Sb_3 particles enhances the high-temperature thermoelectric properties of the composite system. Moreover, one can see that the resistivity ρ decreases obviously with increasing Zn_4Sb_3 content (except $f = 5$ vol.% in the range of 415–600 K). For instance, at room temperature ρ decreases from 6.25×10^{-5} Ω m for $f = 5$ vol.% to 2.25×10^{-5} Ω m for $f = 10$ vol.% and then to 1.55×10^{-5} Ω m for $f = 15$ vol.%.

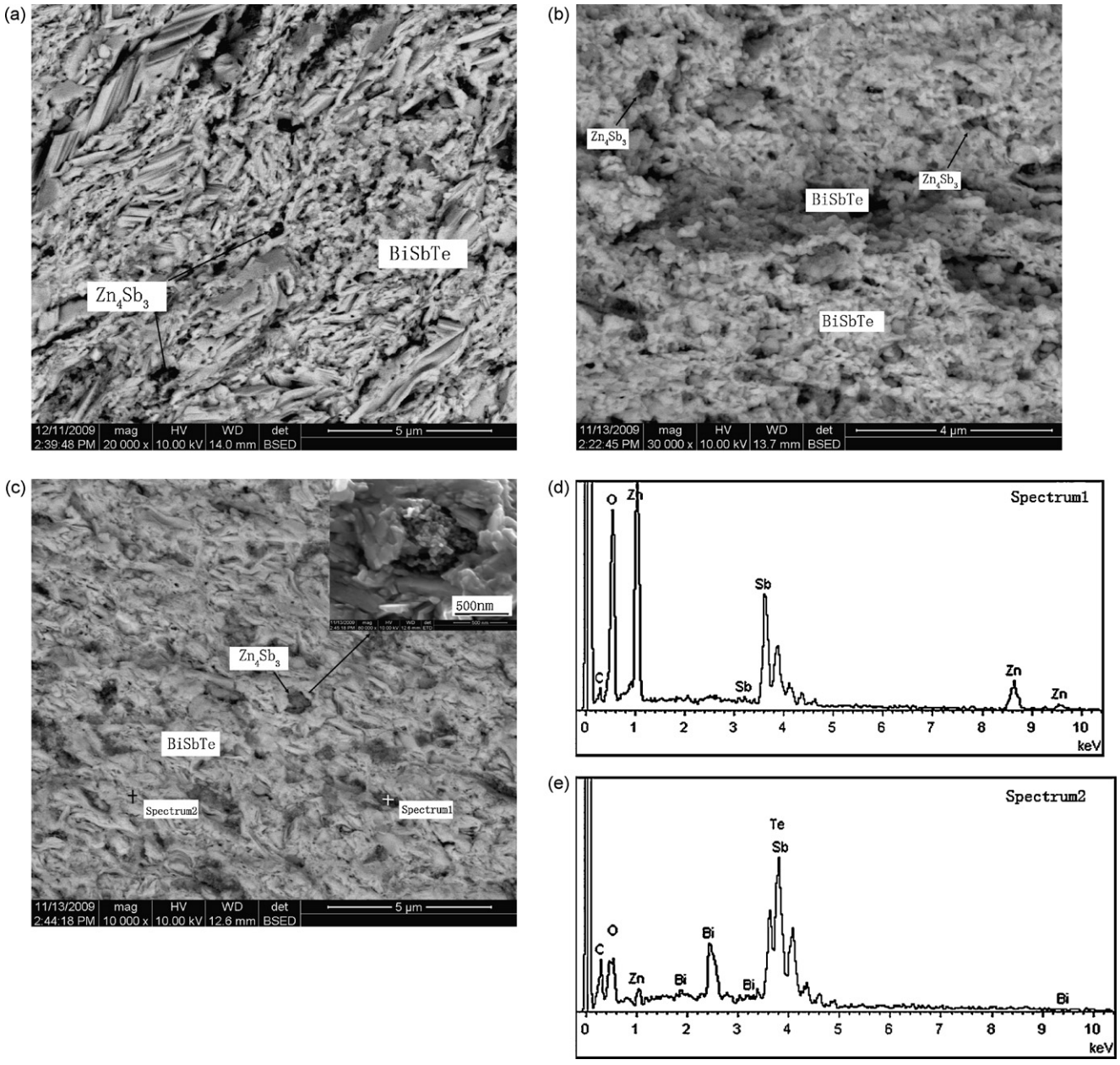

Fig. 3. The back-scattered electron (BSE) images of the fracture surfaces for samples 5 vol.% $(Zn_4Sb_3)/Bi_{0.5}Sb_{1.5}Te_3$ (a), 10 vol.% $(Zn_4Sb_3)/Bi_{0.5}Sb_{1.5}Te_3$ (b) and 15 vol.% $(Zn_4Sb_3)/Bi_{0.5}Sb_{1.5}Te_3$ (c). The inset in (c) is a magnified (secondary electron) image for the agglomerate as indicated in (c). (d) The electron energy spectrum obtained by using EDX for Zn_4Sb_3 phase (black spots as shown in (c)) and (e) is the spectrum for $Bi_{0.5}Sb_{1.5}Te_3$ phase (white background as shown in (c)).

The temperature dependences of Seebeck coefficient for $f(Zn_4Sb_3)/Bi_{0.5}Sb_{1.5}Te_3$ (f = 0, 5, 10 and 15 vol.%) nanocomposites are shown in Fig. 5. The positive values of the S mean that all of the nanocomposite samples belong to p-type semiconductors. In addition, the temperature dependences of Seebeck coefficient for all the samples are similar: they decrease monotonically with decreasing temperature. Generally, Seebeck coefficient of $f(Zn_4Sb_3)/Bi_{0.5}Sb_{1.5}Te_3$ (f = 5, 10 and 15 vol.%) decreases with increasing Zn_4Sb_3 content and S of composite samples is smaller than that of $Bi_{0.5}Sb_{1.5}Te_3$ below a certain temperature. But, Seebeck coefficient of the composite samples becomes larger than that of $Bi_{0.5}Sb_{1.5}Te_3$ at $T > \sim 375$, ~ 425 and ~ 470 K for f = 5, f = 10 and f = 15, respectively. Present results indicate that Seebeck coefficient of the composite system is substantially improved at the high-temperatures due to addition of the dispersed Zn_4Sb_3 particles.

The electrical resistivity of a conventional composite material is determined by the resistivity of both its matrix and dispersed phase(s). However, it is difficult to estimate theoretically the resistivity of our nanocomposite samples from the resistivity of their constituent phases. In fact, we have tried to calculate the resistivity of $f(Zn_4Sb_3)/Bi_{0.5}Sb_{1.5}Te_3$ (f = 5, 10 and 15 vol.%) using the resistivity of Zn_4Sb_3 and $Bi_{0.5}Sb_{1.5}Te_3$ in terms of several formulae for estimating the resistivity of a composite material (such as the rule of mixture) [23]. But, none of the formulae can yield a result that is compared to experimental results as presented above. Actually, all of the predicted values are higher than corresponding magnitudes obtained experimentally. This suggests that the lower resistivity of the composites $(Zn_4Sb_3)/Bi_{0.5}Sb_{1.5}Te_3$ cannot be interpreted by the theory for conventional composites. This is understandable considering that the theory to predict the resistivity of conventional composites assumes no interaction between a

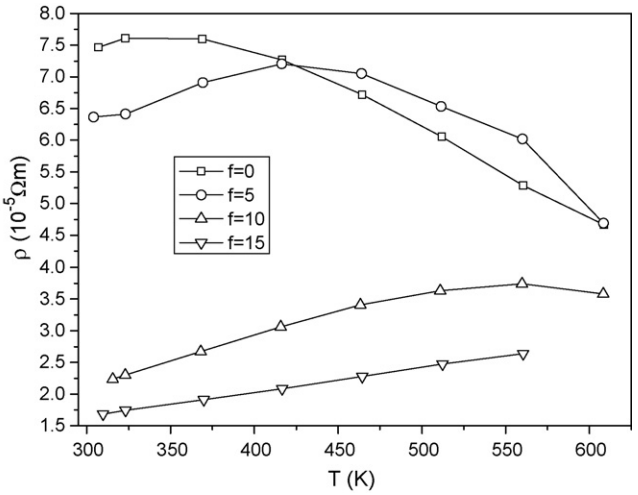

Fig. 4. The temperature dependence of the electrical resistivity ρ for $f(Zn_4Sb_3)/Bi_{0.5}Sb_{1.5}Te_3$ (f = 0, 5, 10 and 15 vol.%).

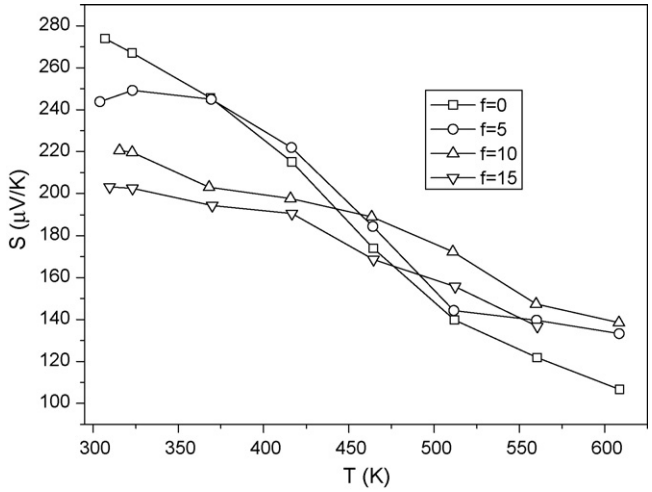

Fig. 5. Variation of Seebeck coefficient S with temperature for $f(Zn_4Sb_3)/Bi_{0.5}Sb_{1.5}Te_3$ (f = 0, 5, 10 and 15 vol.%).

matrix and a dispersed phase within it. However, one can expect that this assumption will not hold in a nanocomposite system, especially when both the constituent phases belong to semiconductors. It is conceivable that as nanoparticles of p-type Zn_4Sb_3 are embedded in p-type $Bi_{0.5}Sb_{1.5}Te_3$ matrix, p–p-type heterojunctions will form at the phase boundaries. Since the band-gap of the Zn_4Sb_3 (E_g = 1.2 eV) [24] is much larger than that of $Bi_{0.5}Sb_{1.5}Te_3$ ($E_{g,\,300\,K}$ = 0.12 eV) [25], the holes in Zn_4Sb_3 phase would transfer to $Bi_{0.5}Sb_{1.5}Te_3$ matrix so that Fermi level of both phases becomes equivalent, leading to the increase of hole concentration in the matrix. In fact, our Hall coefficient measurements demonstrate that hole concentration increases monotonically from 1.05×10^{19}/cm^3 for f = 0 to 3.08×10^{19}/cm^3 for f = 10 vol.% and to 4.89×10^{19}/cm^3 for f = 15%, respectively, as shown in Table 1. Correspondingly, the carrier mobility does not decline remarkably. Nevertheless, one cannot exclude the possibility that some doping process would occur at the phase boundaries. That is, some Zn^{2+} would replace Bi^{3+} or Sb^{3+} in the boundary regimes, resulting in an increase in hole concentration. Hence, the substantial increase in hole concentration is mainly responsible for the decrease of both the resistivity and Seebeck coefficient. The reason why the resistivity of sample 5 vol.% $(Zn_4Sb_3)/Bi_{0.5}Sb_{1.5}Te_3$ is higher than that of $Bi_{0.5}Sb_{1.5}Te_3$ in the range from 415 to 600 K can be ascribed to the lower onset temperature of mixed conduction in $Bi_{0.5}Sb_{1.5}Te_3$. This means that at the temperatures higher than ~410 K, the electrons in the valence band of $Bi_{0.5}Sb_{1.5}Te_3$ are excited substantially into the conduction band. The contribution of these generated electrons together with that of holes leads to a large drop of its resistivity which is even smaller than that of 5 vol.% $(Zn_4Sb_3)/Bi_{0.5}Sb_{1.5}Te_3$ at the high-temperatures (Fig. 4).

Table 1
The carrier concentrations p, Hall mobility μ obtained at 293 K, thermal conductivity λ at ~300 K for $f(Zn_4Sb_3)/Bi_{0.5}Sb_{1.5}Te_3$ (f = 0, 10 and 15 vol.%).

Sample with f (vol.%)	p (10^{19} cm^{-3})	μ (cm^2/V s)	λ (W K^{-1} m^{-1})	λ_L (W K^{-1} m^{-1})
0	1.05	79.7	1.60	1.50
10	3.08	90.4	1.39	1.04
15	4.89	75.4	1.21	0.77

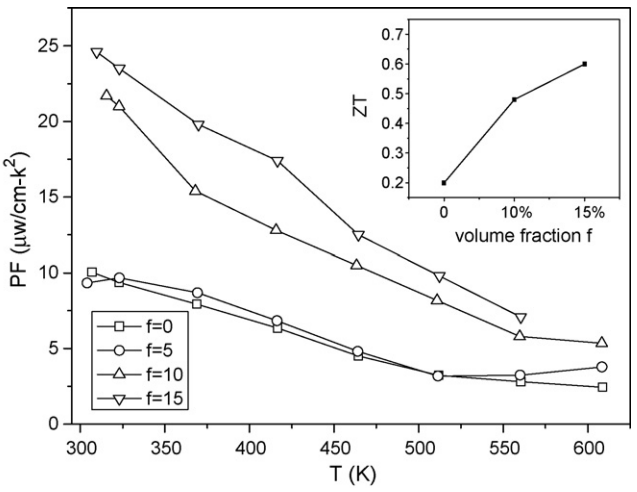

Fig. 6. The temperature dependence of the power factor (PF) for $f(Zn_4Sb_3)/Bi_{0.5}Sb_{1.5}Te_3$ (f = 0, 5, 10 and 15 vol.%). The inset in figure shows the ZT for $f(Zn_4Sb_3)/Bi_{0.5}Sb_{1.5}Te_3$ (f = 0, 10 and 15 vol.%) at room temperature.

3.3. Thermal conductivity and thermoelectric performance

The power factor PF (=S^2/ρ) is given as a function of temperature in Fig. 6. It can be seen that PF of all the samples decreases with increasing temperature. Although PF of 5 vol.% $(Zn_4Sb_3)/Bi_{0.5}Sb_{1.5}Te_3$ is comparable to that of $Bi_{0.5}Sb_{1.5}Te_3$, PF of the other nanocomposite samples with f = 10 and 15 vol.% is much larger than that of $Bi_{0.5}Sb_{1.5}Te_3$ in the whole temperature range investigated in this study, which comes mainly from their much lower resistivity. For instance, PF of the nanocomposite sample with f = 15 vol.% reaches a maximum 25 μW/cm K^2 at ~300 K, which is around 2.5 times larger than that of $Bi_{0.5}Sb_{1.5}Te_3$ at the same temperature. Present results show that the thermoelectric properties of $Bi_{0.5}Sb_{1.5}Te_3$ can be enhanced effectively by the dispersion of nanometer-sized Zn_4Sb_3.

The total thermal conductivity λ of $f(Zn_4Sb_3)/Bi_{0.5}Sb_{1.5}Te_3$ (f = 0, 10 and 15 vol.%) nanocomposites is measured at room temperature, and the obtained result is shown in Table 1. One can see that the total thermal conductivity of nanocomposites $Zn_4Sb_3/Bi_{0.5}Sb_{1.5}Te_3$ reduces remarkably as compared with that of $Bi_{0.5}Sb_{1.5}Te_3$, and the more the Zn_4Sb_3 content, the lower the total thermal conductivity. Total thermal conductivity can be expressed by the sum of a lattice component (λ_L) and a component of mobile charge carriers (λ_C) as: $\lambda = \lambda_L + \lambda_C \cdot \lambda_C$ can be estimated from Wiedemann–Franz's law as $\lambda_C = L_0 T/\rho$ (here L_0 (=2.44×10^{-8} V^2/K^2 for free electrons) and ρ are the Lorenz number and the electrical resistivity, respectively). Consequently, lattice thermal conductivity λ_L can be obtained from

λ and λ_C, as is also listed in Table 1. One can see that thermal conductivity of all the samples comes mainly from their lattice thermal conductivity. Moreover, with increasing Zn_4Sb_3 content the lattice thermal conductivity of the composite samples decreases monotonically from 1.50 $W m^{-1} K^{-1}$ for f = 0–1.04 $W m^{-1} K^{-1}$ for f = 10 vol.% and then to 0.77 $W m^{-1} K^{-1}$ for f = 15 vol.%. Obviously, this decrease of λ_L can be ascribed to the enhancement of phonon scattering by nanometer-sized Zn_4Sb_3 particles as well as the phase boundaries in $Bi_{0.5}Sb_{1.5}Te_3$ matrix.

Based on the data of both power factor shown in Fig. 6 and λ in Table 1, ZT of $f(Zn_4Sb_3)/Bi_{0.5}Sb_{1.5}Te_3$ (f = 0, 10 and 15 vol.%) is then obtained at room temperature, which is shown in the inset of Fig. 6. It can be seen that ZT of the nanocomposites is larger than that of $Bi_{0.5}Sb_{1.5}Te_3$, and it increases with increasing Zn_4Sb_3 content. In particular, ZT of 15 vol.% $(Zn_4Sb_3)/Bi_{0.5}Sb_{1.5}Te_3$ reaches 0.6 at ~300 K, which is about 3-fold increase as compared to that of $Bi_{0.5}Sb_{1.5}Te_3$ obtained in this study. Obviously, this improvement of the thermoelectric properties of $f(Zn_4Sb_3)/Bi_{0.5}Sb_{1.5}Te_3$ (f = 10 and 15 vol.%) originates mainly from the decrease in both thermal conductivity and resistivity, which can be respectively ascribed to the increase of hole concentration and enhanced phonon scattering due to nanometer-sized Zn_4Sb_3 particles embedded in $Bi_{0.5}Sb_{1.5}Te_3$ matrix.

4. Conclusions

The thermoelectric properties of nanocomposites $f(Zn_4Sb_3)/Bi_{0.5}Sb_{1.5}Te_3$ (f = 0, 5, 10 and 15 vol.%) have been studied at temperatures from 300 to 650 K. The results indicate that the resistivity and Seebeck coefficient of $f(Zn_4Sb_3)/Bi_{0.5}Sb_{1.5}Te_3$ (f = 0, 5, 10 and 15 vol.%) decreases with increasing Zn_4Sb_3 content, which is mainly caused by the increase in carrier concentration after dispersion of nanometer-sized Zn_4Sb_3 particles. Experiments also show that room temperature thermal conductivity of $f(Zn_4Sb_3)/Bi_{0.5}Sb_{1.5}Te_3$ decreases monotonically with increasing f due to enhanced phonon scattering by the dispersed Zn_4Sb_3 nanoparticles and the phase boundaries. Moreover, 15 vol.% $(Zn_4Sb_3)/Bi_{0.5}Sb_{1.5}Te_3$ exhibits the largest power factor (25 $\mu W/cm K^2$ at ~300 K) that is 2.5 times larger than that of $Bi_{0.5}Sb_{1.5}Te_3$. Correspondingly, its figure of merit (ZT = 0.6 at ~300 K) is about three times larger than that of $Bi_{0.5}Sb_{1.5}Te_3$. Present results indicate that the thermoelectric properties of $Bi_{0.5}Sb_{1.5}Te_3$ can be enhanced effectively by the dispersion of nanometer-sized Zn_4Sb_3.

Acknowledgement

Financial support from National Natural Science Foundation of China (Nos. 10774145, 50701043 and 10904144) is gratefully acknowledged.

References

[1] D.M. Rowe, CRC Handbook of Thermoelectrics, CRC Press, LLC, 1995.
[2] D.Y. Chung, T. Hogan, P. Brazis, R.L. Melissa, Science 287 (2000) 1024–1027.
[3] A.A. Joraide, J. Mater. Sci. 30 (1995) 744–748.
[4] J. Seo, K. Park, D. Lee, C. Lee, Mater. Lett. 35 (1998) 4–9.
[5] P. Pierrat, A. Dauscher, B. Lenoir, R. Martin-lopez, H. Scherrer, J. Mater. Sci. 32 (1997) 3653–3657.
[6] J. Zhou, S. Li, H.M.A. Soliman, M.S. Toprak, M. Muhammed, D. Platzek, E. Muller, J. Alloys Compd. 471 (2009) 278–281.
[7] L.D. Zhao, B.P. Zhang, W.S. Liu, H.L. Zhang, J.F. Li, J. Alloys Compd. 467 (2009) 91–97.
[8] C.H. Kuo, C.S. Hwang, M.S. Jeng, W.S. Su, Y.W. Chou, J.R. Ku, J. Alloys Compd. (2010) 171, doi:10.1016/jallcom.2010.02.171.
[9] C.D. Moon, S. Shin, D.H. Kim, T.S. Kim, J. Alloys Compd. (2008) 114, doi:10.1016/j.jallcom.2010.03.114.
[10] Q. Yao, Y.J. Zhu, L.D. Chen, Z.L. Sun, X.H. Chen, J. Alloys Compd. 481 (2009) 91–95.
[11] R. Venkatasubramanian, E. Siivola, T. Colpitts, B. O'Quinn, Nature 413 (2001) 597–602.
[12] M. Takashiri, S. Tanaka, K. Miyazaki, H. Tsukamoto, J. Alloys Compd. 490 (2010) L44–L47.
[13] B. Poudel, Q. Hao, Y. Ma, Y.C. Lan, A. Minnich, B. Yu, X. Yan, D.Z. Wang, A. Muto, D. Vashaee, X.Y. Chen, J.M. Liu, M.S. Dresselhaus, G. Chen, Z.F. Ren, Science 320 (2008) 634–638.
[14] Y.Q. Cao, T.J. Zhu, X.B. Zhao, X.B. Zhang, J.P. Tu, Appl. Phys. A 92 (2008) 321–324.
[15] L. Zhou, X. Zhang, X. Zhao, C. Sun, Q. Niu, J. Alloys Compd. (2008), doi:10.1016/j.jallcom. 2010.01.024.
[16] J. Martin, L. Wang, L.D. Chen, G.S. Nolas, Phys. Rev. B 79 (2009) 115311–115315.
[17] W.W. Zhou, J.X. Zhu, D. Li, H.H. Hng, F.Y.C. Boey, J. Ma, H. Zhang, Q.Y. Yan, Adv. Mater. 21 (2009) 3196–3200.
[18] X.A. Fan, J.Y. Yang, Z. Xie, K. Li, W. Zhu, J. Phys. D: Appl. Phys. 40 (2007) 5975–5979.
[19] Y.Q. Cao, X.B. Zhao, T.J. Zhu, X.B. Zhang, J.P. Tu, Appl. Phys. Lett. 92 (2008) 143106–143109.
[20] T. Caillat, J.P. Fleurial, A. Borshevsky, J. Phys. Chem. Solids 58 (1997) 1119–1125.
[21] M. Chitroub, F. Besse, H. Scherrer, J. Alloys Compd. 460 (2008) 90–93.
[22] K. Ueno, A. Yamamoto, T. Noguchi, T. Inoue, S. Sodeoka, H. Takazawa, C.H. Lee, H. Obara, J. Alloys Compd. 384 (2004) 254–260.
[23] P.S. Liu, T.E. Li, C. Fu, Mater. Sci. Eng. A 268 (1999) 208–215.
[24] M. Tapiero, S. Tarabichi, J.G. Gies, C. Nognest, J.P. Zielinger, M. Jouda, J. Loison, M. Robino, Sol. Energy Mater. 12 (1985) 257–274.
[25] B.M. Gol'tsman, V.A. Kutasov, L.N. Luk'yanova, Phys. Solid State 50 (2008) 235–236.